Perturbation-induced droplets (PiD) for manipulating droplet structure and configuration in microfluidics

Jingmei Li[1,2], Nitesh Mittal[2], Sze Yi Mak[1,2], Yang Song[1,2], Ho Cheung Shum[1,2]*

[1]HKU-Shenzhen Institute of Research and Innovation (HKU-SIRI), Shenzhen, Guangdong, China

[2]Department of Mechanical Engineering, University of Hong Kong, Hong Kong

*Corresponding Author: ashum@hku.hk

KEYWORDS: Perturbation-induced droplets, on-demand sizes, on-demand structure, interfacial tension, droplet-based microfluidics

ABSTRACT

In this work, we mechanically perturb a liquid-in-liquid jet to manipulate the size and structure of the droplets formed from breakup of the jet. The induced breakup is relatively insensitive to fluctuations in the surrounding fluid flow. When the amplitude of perturbations is large and the interfacial tension of the liquid-liquid system is low, the size of the droplets can be precisely tuned by controlling the rate at which the liquid exits the tip of the dispensing nozzle through the

frequency of perturbation. When applied to microfluidic devices with the appropriate geometry, our approach of perturbation-induced droplet (PiD) offers a strategy to manipulating droplet structures. We demonstrate that, by varying the imposed perturbation frequency and phase lag, the structure of the multi-compartmental drops and the configuration of the resultant drops in the same flow condition can be manipulated. Moreover, after careful treatment of the wettability of the devices, we show that the structure of the droplets can be precisely controlled to change from single emulsion to double emulsion within the same device. The perturbation-induced droplet generation represents a new paradigm in the engineering of droplets, enhancing current droplet-based technologies for applications ranging from particle fabrication to confined micro-reactions.

1 INTRODUCTION

The increasing need for the use of smaller amount of fluids in biological assays and microchemistry is met by the rapid developments in microfluidic technologies. For example, microfluidic platforms can be used to diagnose malaria.[1] Micro-bubbles generated in microfluidic devices can be used to enhance the efficiency of oxidation process of tetrahydro-2-ethylanthrahydroquinone (THEAQH2).[2] Micro-particles with different color components can be used for display.[3] Among the widely used microfluidic technologies, droplet-based microfluidics, which refers to the use of droplets prepared in microfluidic devices as micro-reactors, [4, 5, 6] as sample carriers for biological analysis and therapeutic agents,[7, 8, 9, 10] and as templates for advanced materials,[11, 12, 13] advances the efficiency in chemical and biological reactions, speed and accuracy of biological analysis, and performance in materials applications. Different microfluidic approaches have been devised to manipulate droplets, such as electro-wetting-based digital microfluidics[10, 14, 15] and continuous-flow-based droplet microfluidics,

which is the focus of the current work. To facilitate the use of droplet-based microfluidics for such applications, the size and structure of the droplets must be tailored according to the needs of the applications. There are numbers of work to study the mechanism of droplet generation and liquid breaking up during continuous operation.[16, 17, 18] In principle, the size and the structure of droplets are decided by the fluid properties,[19, 20] such as the interfacial tension[21] between the two immiscible fluids and their viscosities,[22, 23] as well as controlling parameters, including flow rates,[20, 24, 25] driving pressure[26] and device geometries.[27, 28] Practically, droplet size is controlled by varying the flow rates or the driving pressure of the fluids. For instance, in co-flow and flow-focusing droplet makers, the size of droplets decreases with decreasing flow rate of the inner fluid and increasing the flow rate of the outer fluid.[18, 19, 29] The structure of the droplets can also be manipulated by changing the flow rate ratio of the different emulsion phases involved.[30, 31, 32] In the generation of double emulsions, the number of cores in core-shell droplets increases with increasing ratio of the flow rates between the core and shell phases as well as that between the shell and continuous phases.[32] To prepare droplets with well-defined sizes and structure, highly stable liquid dispensing systems, such as precision syringe pumps[33] and pressure regulators, are needed for controlling the flow rates and the driving pressure. Over the past decade, some components, such as valves and micro-actuators, are used to achieve on-demand generation of droplets with different sizes,[34, 35, 36] as reported in some experimental studies[37, 38, 39] and theoretical studies.[40, 41, 42] In particular, one promising approach is to introduce perturbation, for instance, by incorporating piezoelectric actuators,[35, 43] squeezing the tubing that delivers the fluids using a mechanical vibrator,[39, 44] adjusting the driving pressure of the fluids using valves,[34, 45] and introducing surface acoustic waves through on-device transducers.[46, 47] These perturbations have been applied to different systems, such as all-aqueous droplets[39, 48] with ultra-

low interfacial tension, as well as gas-in-liquid bubbles,[36] with high interfacial tension. The sensitivity of the interfaces towards perturbations varies with their interfacial tension; nevertheless, on-demand control over droplet size with fast response[49, 50] can be achieved by adjusting the perturbation amplitude,[35, 51] or frequency.[42] While on-demand change in droplet sizes has been demonstrated, it remains difficult to change the entire structure of droplets, for instance from single ones to multi-compartmental ones with tunable number of compartments, or to core-shell ones with tunable core size within the same device during continuous operation. A new approach that allows continuous generation of droplets with on-demand control over sizes and structures will present a new paradigm in the engineering of droplets.

In this paper, we introduce a versatile approach based on hydrodynamic perturbation to prepare droplets allowing on-demand change in droplet size as well as its structure. In the first part, we demonstrate its capability in generating droplets with on-demand changes in sizes. The approach is highly robust and the droplet size can be largely maintained despite changes in the flow rates of the continuous phase. It is particularly effective for emulsion systems with a low interfacial tension for high-amplitude perturbations. In the second part, the perturbation-induced droplets (PiD) approach can be adopted to allow adjustment of the droplet structures during continuous generation. Introducing two neighboring droplet phases using two parallel injection channels, multi-compartmental droplets can be generated with the PiD approach. The ratio of compartment of two droplet phases can be controlled by applying different perturbation frequencies to the two liquid phases. Configurations of droplets can be further controlled by tuning the phase lag between the applied perturbations. Besides multi-compartmental droplets, PiD approach can realize switching from single emulsion droplets to core-shell droplets with adjustable size of the

cores during a continuous operation. The PiD approach enhances current droplet-based technologies for applications ranging from particle fabrication[11] to confined micro-reactions[6].

2 EXPERIMENTAL SECTION

2.1 Materials and Methods

Glass micro-capillary device, fabricated by aligning two tapered glass capillaries (World Precision Instruments, Inc. 1B150F-6) with different tip diameters against each other has been used in this study (Figure 1). The capillary is tapered using a micro-pipet puller (P-97, Sutter). To generate single emulsion, the glass capillary with the smaller tip diameter (d_S=50±5 μm as its outer diameter) is used for injecting the jet phase whereas the glass capillary with the larger tip (d_L=450±30 μm as its inner diameter) is used for collecting the generated droplets. Both capillaries are fitted into a square capillary with an inner dimension of 1500 μm. The geometry of the device is axisymmetric. The schematic diagram of the experimental setup is shown in Figure 1 (A). To generate bi-compartmental Janus emulsion droplets and multi-compartmental droplets, a glass capillary with two parallel channels (World Precision Instruments, Inc. TST150-6) is used to inject two neighboring jet phases, as shown in Figure 1 (B). The wettability of the wall of injection tip affects the resultant structure of the drop, as shown in Figure 1 (C). We altered the wettability of glass capillary (World Precision Instruments, Inc. 1B100F-6) from hydrophilic to hydrophobic by treating it with octadecyl trimethoxysilane (Aldrich). By doing so, emulsion structures can be easily switched from single to core-shell using the PiD approach.

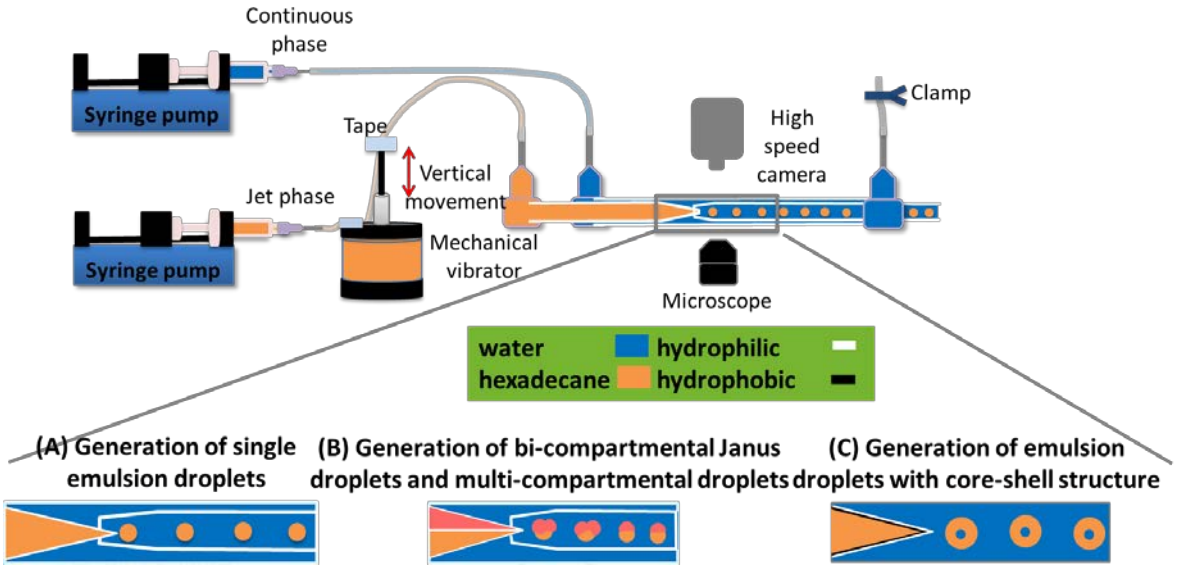

Figure 1 Schematic of the experimental setup for the generation of droplets. (A) Generation of single emulsion droplets. (B) Generation of bi-compartmental Janus droplets and multi-compartmental droplets. (C) Generation of emulsion droplets with a core-shell structure. Solutions are delivered to glass capillary microfluidic devices with a co-flow geometry. A mechanical vibrator is used to vibrate the plastic tubing to deliver the inner fluid and this introduces hydrodynamic perturbation to the system.

Syringe pumps (Longer pump, LSP01-2A) are used to inject the fluids into the device at stable and controllable flow rates. In devices with co-flow geometries, both fluids flow in the same direction. Different combinations of surfactants are added to hexadecane-in-water emulsion system to vary the interfacial tension. The interfacial tension is measured using a spinning drop tensiometer (SITE100, Kruss) as shown in Table 1. To generate Janus droplets, we use three immiscible solutions, including hexadecane (Sigma Aldrich) with 0.85 wt. % Span 80 and tripotassium phosphate (K_3PO_4)-rich phase as the two jet phases, and polyethylene glycol (PEG, M_W=8000) (Sigma Aldrich)-rich phase as the continuous phase. The two immiscible aqueous phases are prepared by dissolving 10 wt. % tripotassium phosphate (K_3PO_4) and 16 wt. %

polyethylene glycol (PEG, M_W=8000) (Sigma Aldrich) in water, followed by centrifugation (Labnet, Spectrafuge 6c compact) at 6000 rpm for 6 minutes. After the mixture separates into two bulk phases, we extract the K_3PO_4-rich bottom phase and PEG-rich top phase, as one of the jet phase and continuous phase respectively. Water-in-oil-in-water and oil-in-water-in-oil double emulsions are produced with hexadecane as the oil phase and water with 2 wt. % SDS as the aqueous phase.

Jet Phase	Continuous Phase	Interfacial Tension (mN/m)
Hexadecane	Water with 2 wt. % SDS	5.5±0.2
Hexadecane	Water with 10 wt. % Tween 20	2.3±0.3
Hexadecane with 0.85 wt. % Span 80	Water with 10 wt. % Tween 20	0.35±0.05
Hexadecane with 0.85 wt. % Span 80	PEG-rich phase	1.63±0.1
K_3PO_4-rich phase	PEG-rich phase	0.74±0.03

Table 1 Various configurations of fluids used in our study as jet and continuous phases with their corresponding interfacial tension value.

By shaking the tubing of the jet phase vertically, periodic perturbations of pressure are introduced into the flow. The mechanical perturbation is achieved by a mechanical vibrator

(Pasco Scientific, Model SF-9324) (shown in Figure 1) controlled by amplified electrical signals. After measuring the displacement of the vibrator by a laser sensor (MICRO-EPSILON), we confirmed that the frequency of vibration was the same as the frequency of the electrical signal, and the amplitude of the displacement of the vibrator increases with increasing amplitude of the electrical signals, as shown in Figure 2.

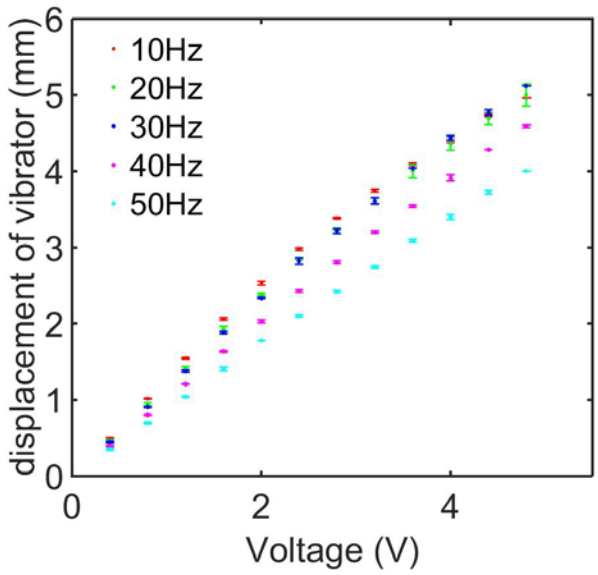

Figure 2 Displacement of the mechanical vibrator used in our study as a function of the voltage applied for various vibration frequencies.

2.2 Characterization of the perturbation-induced droplet formation

In our PiD approach, the direction of the flow of the jet phase oscillates, due to the mechanical perturbation imposed. Within each cycle of perturbation, when the driving pressure, which is the pressure difference across the micro-channel, is positive, the jet phase flows downstream. A hemispherical drop attached to the injection tip is formed as soon as the jet phase is pushed out from the injection tip. The effect of the shear force from the outer liquid phase is very weak, as

the Capillary number of the outer phase, which is defined as the ratio between shear effect and surface tension effects, ranges from around 0.01 to 0.1. Therefore, the hemispherical drop does not detach from the jet phase; instead, it remains attached to the jet phase via a thin liquid bridge, as shown in Figure 3 (A3, A4). During the transition from a positive driving pressure to a negative one, the liquid is abruptly withdrawn from the liquid bridge that connects the bulk jet phase in the nozzle and the hemispherical drop, resulting in a decrease of the jet diameter. When the diameter gets sufficiently small, the jet breaks up to form droplets (Figure 3 (A)). To better understand the process of droplet generation, we measure the distance from jet-outer interface to the injection tip to show the movement of jet phase, as shown in Figure 3 (B). When jet phase breaks into droplets, the value of this distance will change from positive to negative. In the rest part of our paper, we also use the distance changed with time to present the process of droplet generation.

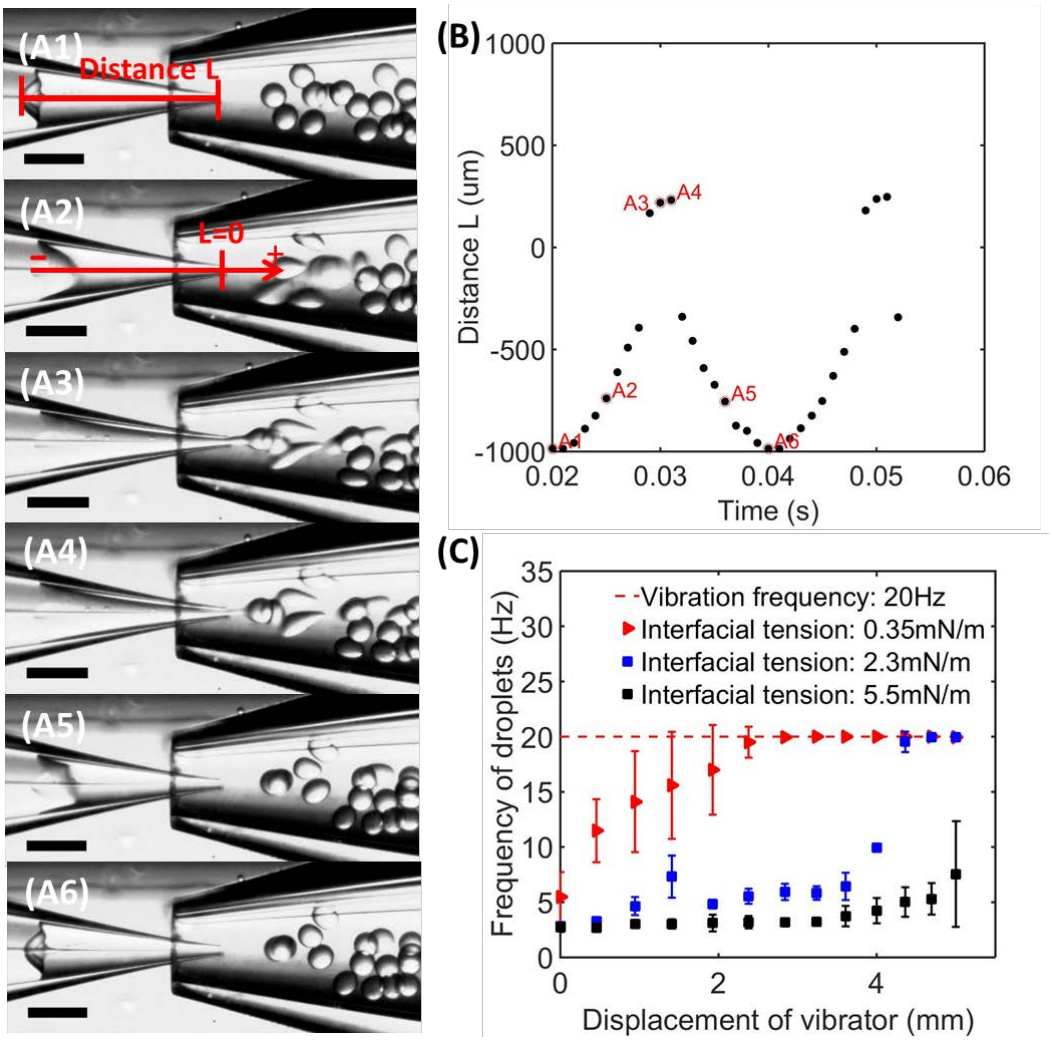

Figure 3 Generation of droplets with the proposed PiD approach. Scale bars are 300 μm (A) A positive driving pressure pushes the jet phase downstream whereas a negative driving pressure leads to retraction of the jet phase back into the nozzle. The applied frequency here is 50 Hz; (B) distance from the jet-outer interface to the injection tip measured based on Figure 3 (A). (C)The frequency of droplets generation at various amplitudes and interfacial tensions. The frequency of vibrator here is 20 Hz. The frequency of droplets is collected by counting the number of droplets generated within 4.25 s and the error bars are obtained by averaging the results from 9 sets of experiments.

2.3 Effect of perturbation amplitude on droplet generation at different interfacial tension

With a low amplitude of perturbation, the frequency of droplet generation is close to its natural generation frequency, which is the frequency of droplet generation without perturbation, as indicated by the frequencies at a displacement of zero in Figure 3 (C). When the perturbation amplitude increases, for instance, from a vibrator displacement of 1 mm to 5mm, the frequency of droplet generation increases and becomes closer to the frequency of perturbation (Figure 3 (C)). The withdrawal of liquids from the jet prompts the breakup of droplets in the period of the perturbation cycle with a negative driving pressure. With a low amplitude of perturbation, the bridge cannot get sufficiently thin during each cycle of perturbation to trigger the breakup of jet, resulting in a lower and less defined frequency of generation of droplets. As the rate at which the fluid is withdrawn from the jet increases with increasing amplitude of perturbation, above a certain threshold amplitude, the frequency of droplet generation becomes directly controlled by the perturbation frequency. For instance, with an interfacial tension of 2.3 mN/m, two cycles of perturbations result in the generation of one droplet at a perturbation amplitude of around 4 mm; thus, the frequency of droplet generation (~10 Hz) is half of the frequency of perturbation (20 Hz), as indicated by the blue square symbols in Figure 3 (C). When the amplitude increases to 4.7 mm or above, one droplet can be generated within each cycle of perturbation; thus, the frequency of droplets generation is the same as the frequency of perturbation (Figure 3 (C)). Indeed the physical location of the mechanical vibrator with respect to the injection point is critical and affect how the droplets are generated. In our work, we have consistently placed the vibrator in a fixed position near to the inlet of the device to ensure consistency in comparing the different results. In our later experiments, we adjust the amplitude to be the same as or higher than the threshold amplitude to ensure that the frequency of droplet generation is the same as the

frequency of perturbation. All the later discussion in Section 3 is within the amplitude range in which the two frequencies match.

With an increasing interfacial tension, the threshold of amplitude, at which the frequency of droplets generation equals to the frequency of perturbation, increases. This is because a decrease in the jet diameter leads to a corresponding increase in the jet curvature and thus the Laplace pressure $P_{Laplace} = \gamma(1/R)$ increases accordingly, where γ is the interfacial tension, and R is the radius of jet diameter. For a given perturbation amplitude, as the interfacial tension decreases, the resulting jet gets thinner and more likely reaches a threshold diameter that will trigger breakup of the jet. Therefore, the PiD approach is most effective for perturbations with a large amplitude and liquid-liquid systems with a low interfacial tension. When the interfacial tension of the system increases from 0.35 mN/m to 2.3 mN/m, the amplitude threshold increases from 2.8 mm to 4.7 mm approximately. When the interfacial tension is even higher (5.5 mN/m), the target amplitude threshold is beyond the maximum possible amplitude of the vibrator, as indicated by the black squares in Figure 3 (C).

2.4 Control over size of single emulsion drops

By controlling the droplet generation frequency, the size of droplets can be determined based on the flow rate of the jet phase. According to mass conservation, with a constant flow rate of the jet phase, Q_{in}, the total volume of the original jet should be equal to the frequency of droplet generation, F_d, multiplied by the volume of each droplet, V_d, with a diameter D:

$$Q_{in} = V_d * F_d \qquad (1)$$

The channels in our devices are axisymmetric along the flow direction. Hence, the droplet morphology should also be axisymmetric as well. Thus, the circular shape in the two-

dimensional views should be representative in the z-direction as well. Therefore, we assume the droplets to be spherical based on their circular shape in the high-speed microscope images. In this manner, the volume of the droplets, V_d, can be estimated as:

$$V_d = 4/3 \cdot \pi(D/2)^3 \quad (2)$$

Therefore, when F_d is the same as the frequency of perturbation, F_p, the average diameter D of droplets can be predicted by the following expression:[14]

$$D = 2\sqrt[3]{(3Q_{in}/(4F_p\pi))} \quad (3)$$

Based on equation (3), the sizes of droplets depend on the inner flow rate and perturbation frequency. To confirm this, we keep the flow rates of both jet phase and continuous phase constant. Without perturbation, droplets are generated with a diameter of around 350 μm; this is indicated as having a zero value in the perturbation frequency in the plot of droplet diameter as a function of the perturbation frequency in Figure 4 (A). With a 10 Hz perturbation, the size of droplets is reduced to 220 μm. When we further increase the perturbation frequency from 10 Hz to 90 Hz, the size of droplets decreases with increasing perturbation frequency, as shown in Figure 4 (A). The size of the droplets obtained from the experiments agrees very well with the numerical values predicted with the equation, as shown in Figure 4 (B). Moreover, based on the equation (3), the droplet size depends weakly on the flow rate of the continuous phase. To confirm this, we vary the continuous phase flow rate from 2 ml/h to 20 ml/h and measure the resultant droplet size, which remains constant despite changes in the flow rate of the continuous phase (Figure 4 (C)). Thus our PiD approach is robust and allows precise control over the size of droplets. We acknowledge that further increase in the continuous phase flow rate could modify the droplet generation process and change the droplet size. However, in this work, we limit

changes in the continuous phase flow rate to ensure weak dependence of droplet size on the flow rate.

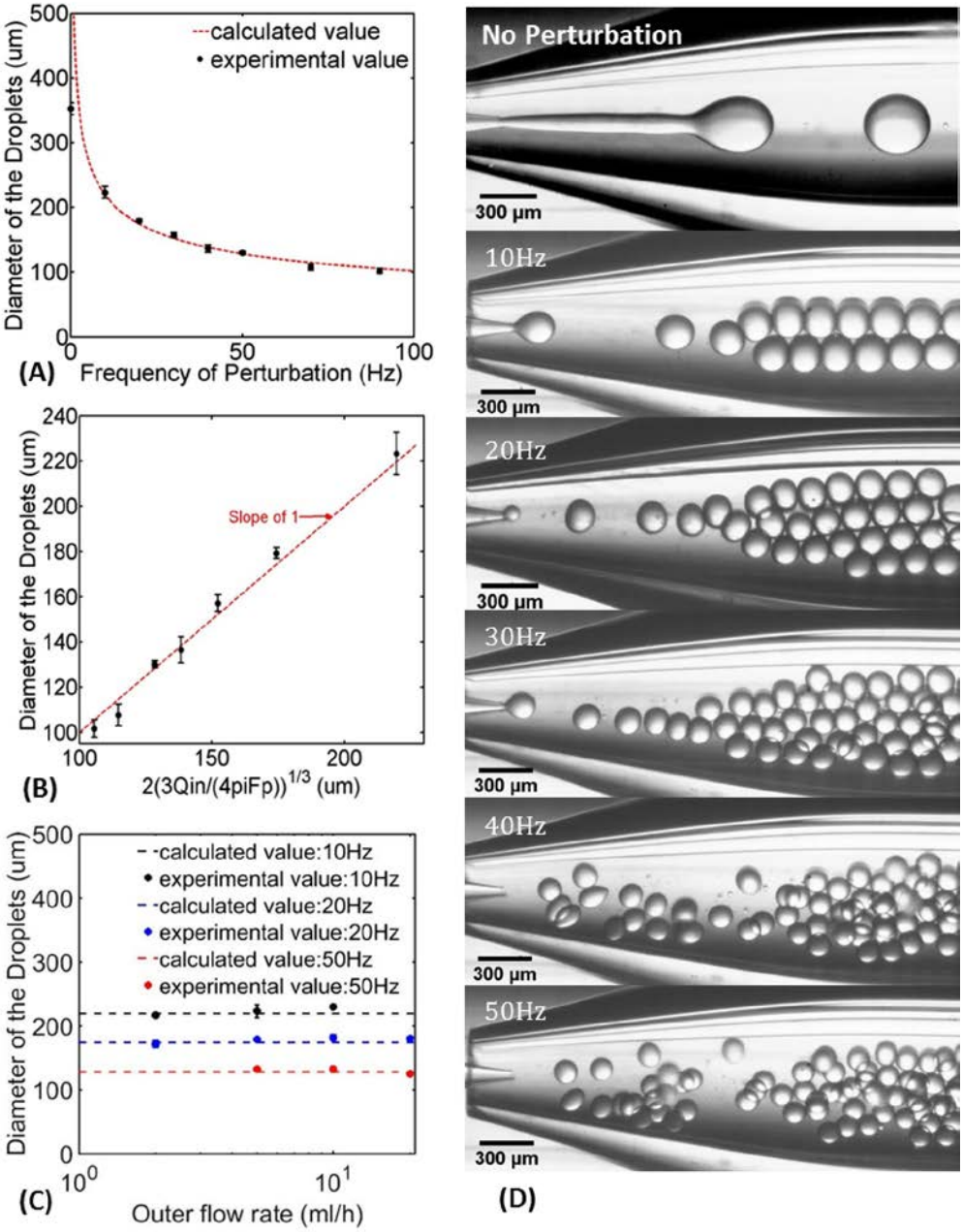

Figure 4 (A) Diameter of the droplets as a function of the frequency of perturbation. A zero perturbation frequency indicates the absence of any applied perturbation. The black dots indicate the experimentally measured values, while the red line indicates the theoretical values calculated

based on equation (3). (B) Measured diameter of the droplets as a function of the calculated value of their diameter. The applied perturbation frequencies are 10 Hz, 20 Hz, 30 Hz, 40 Hz, 50 Hz, 70 Hz and 90 Hz. (C) Diameter of droplets as a function of the outer flow rates at a perturbation frequency of 10 Hz, 20 Hz and 50 Hz. (D) Droplets generated at various frequencies of perturbation (0 Hz, 10 Hz, 20 Hz, 30 Hz, 40 Hz and 50 Hz).

3 RESULTS AND DISCUSSION

In the first part of our results, we show the capability of the PiD approach in generating droplets with on-demand changes in droplet size. Using PiD approach, the size of each individual emulsion droplet can be precisely and instantaneously controlled by the frequency of perturbation. In the second part, we demonstrate the capability of PiD approach in manipulating the structure of droplets during continuous operation. By introducing two neighboring droplet phases, PiD approach can realize generation of bi-compartmental droplets with various structures. The number of the compartments can be easily controlled by varying the two different perturbation frequencies and by imposing a phase lag between the two perturbations. Moreover, by using a device with the appropriate wettability, the droplets generated can be switched from single emulsion droplets to core-shell droplets without the need to switch to a different device or to interrupt the operation. The core-shell ratio can be precisely controlled by varying the amplitude of perturbation.

3.1 PiD approach for generating single emulsions with on-demand changes in droplet sizes

While the size of the droplets can be uniformly controlled, customized tuning of the size distribution of the emulsion requires a quick response of the droplet sizes to changes in perturbation frequency. In conventional droplet microfluidics, it typically takes tens of seconds or even several minutes for droplets to adopt a new steady size after an abrupt change in fluid flow rate. During the transition to the steady size, hundreds of droplets with undesired and uncontrolled diameters are generated. However, with our PiD approach, since the response time of the mechanical vibrator is within a few micro-seconds, the size of droplets can be tuned instantaneously, as shown in Figure 5. To demonstrate this, as we switch off a 50 Hz vibration, the transition from the initially smaller droplets to the subsequently larger droplets is completed within a time shorter than the droplet generation time, resulting in a sharp droplet size change, as shown in Figure 5 (A). We also apply three successive frequencies of 60 Hz, 10 Hz, and 30 Hz; the resultant droplets show corresponding alternation in size (Figure 5 (B)). To highlight the versatility and control, we generate trains of three droplets, each with a uniquely different size by applying single-cycles of perturbations. The resultant droplets synchronize with the applied perturbation and their sizes match the predict values well (Figure 5 (C)). By allowing on-demand changes of droplet sizes, our PiD approach enables preparation of emulsions with customized size distributions.

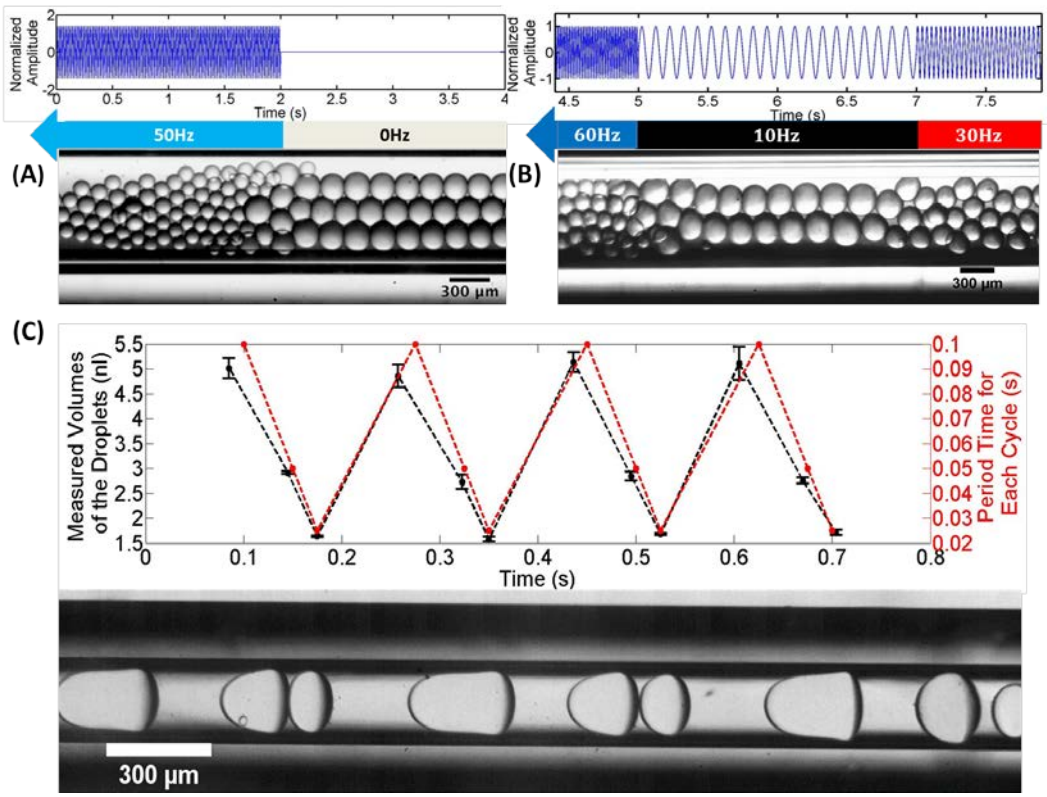

Figure 5 On-demand changes of droplets with our PiD approach. (A) Change in droplet size after switching off a 50 Hz perturbation. The flow rate of the jet phase is 200 µl/h. The arrow indicates the direction of flow. (B) Change in droplet size in response to three successive perturbations with frequencies of 60 Hz, 10 Hz and 30 Hz respectively. The flow rate of jet phase is 400 µl/h. The arrow indicates the direction of flow. (C) Change in the sizes of trains of three droplets responding to single-cycle perturbations with frequencies of 10 Hz, 20 Hz and 40 Hz respectively. Volumes of the droplets measured by image processing are shown as black dots with error bars and the periods of each cycle of perturbations are shown as red dots.

3.2 PiD approach for manipulating the structure of droplets during continuous operation

3.2.1 PiD approach for synchronizing formation of droplets, enabling generation of bi-compartmental Janus droplets

Besides the control of droplet sizes, the PiD approach also facilitates the manipulation of droplet structures. When the device for making single emulsion is modified to allow parallel injection of two neighboring jet phases, bicompartmental droplets can be induced by our PiD approach, with the same level of control over their sizes (Figure 6 (A)). In the absence of any perturbation, due to the difference in fluidic and interfacial properties, such as viscosity and interfacial tension, it is difficult to synchronize the breakup of the two jets into droplets and achieve a uniform droplet generation frequency for Janus droplets. This is exacerbated in systems with ultra-low interfacial tension, where even a single jet breaks up in an uncontrolled manner into droplets with non-uniform sizes.[39] By contrast, when the breakup is induced by an applied perturbation, droplets break up at the same frequency determined by the perturbation. To demonstrate the synchronized generation of pairs of droplets, we use hexadecane and a tripotassium phosphate (K_3PO_4) solution as the two jet phases and polyethylene glycol (PEG) solution as the continuous phase. In the absence of perturbation, the K_3PO_4 jet breaks up in an unstable manner at a frequency ranging from 10 Hz to 11 Hz, while the hexadecane jet breaks up into uniform droplets at a frequency of around 35 Hz. As the generation of the two types of droplets is unsynchronized, the resulting droplets vary vastly in size, shape and structure, as shown in Figure 6 (B1). By attaching both pieces of tubing that are used to deliver the two jet phases to a mechanical vibrator, perturbations with the same frequency are introduced to the system. This forces the breakup of the two jets to be synchronized at the perturbation frequency, allowing controlled generation of Janus droplets with a uniform size, which decreases with increasing perturbation frequency, as shown in Figure 6 (B2 & B3).

3.2.2 PiD approach for manipulating the structure of multi-compartmental droplets

Apart from synchronizing perturbations of the same frequency to generate Janus droplets, different perturbation frequencies can be applied to the two droplet phases, a tripotassium phosphate (K_3PO_4) solution and hexadecane, achieving multi-compartmental droplets with different structures, as shown in Figure 6 (B4, B5 & B6). When the frequency of the liquid phase 1 (K_3PO_4 solution) doubles that of the liquid phase 2 (hexadecane), multi-compartmental drops with two droplets of liquid phase 1 connected to a droplet of liquid phase 2 can be generated (Figure 6 (B4)). When the ratio of perturbation frequencies between phase 1 and phase 2 is modified to 1:2, drops with one phase 1 droplet and two phase 2 droplets can be prepared, as shown in Figure 6 (B5). A further increase in the frequency of the phase 2 to attain a frequency ratio of 1:3, will result in drops combined with one phase 1 droplet and three phase 2 droplets (Figure 6 (B6)). The ratio of compartment of the two droplet phases is equal to the ratio of perturbation frequencies applied. The PiD approach shows its capability in manipulating configuration of droplets by varying the ratio of the frequencies of the two applied perturbations.

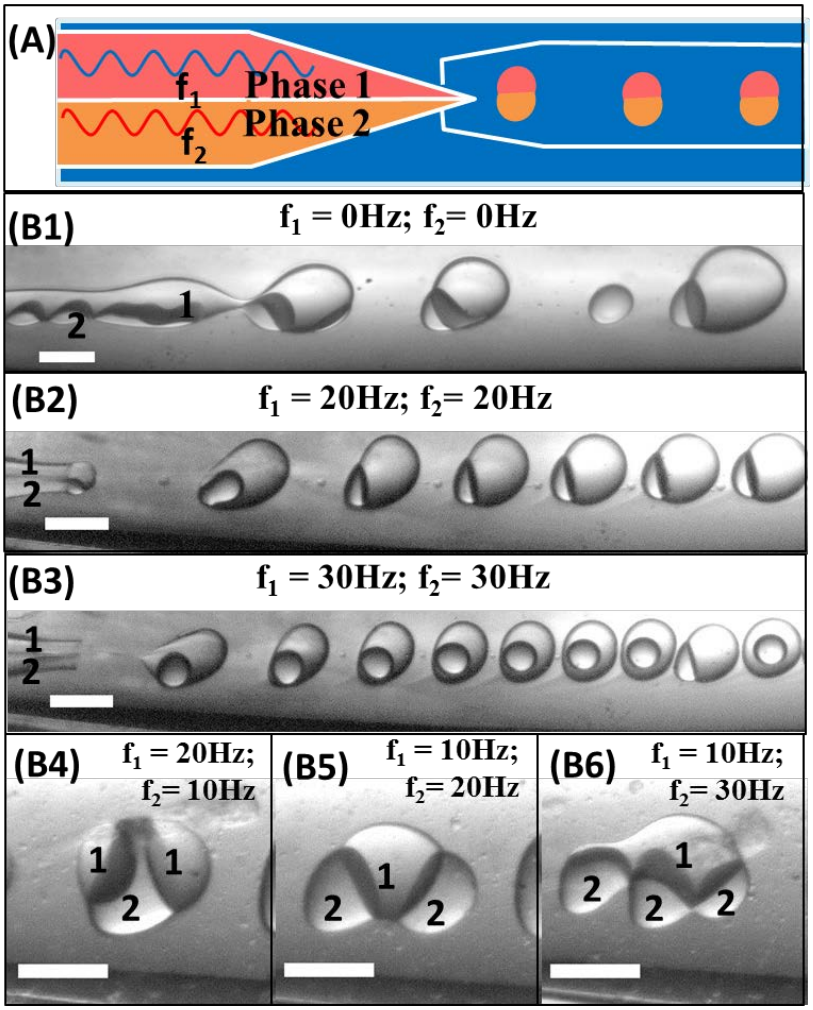

Figure 6 Generation of bicompartmental droplets. (A) Schematic of bi-compartmental droplet generation using a parallel injection tip. Phase 1 is K_3PO_4 solution while phase 2 is hexadecane with 0.85 wt. % Span 80. (B) Droplets generated under different combination of perturbation frequencies. (B1) Without perturbation, droplet structures are not stable; the generation frequencies (f_1, f_2) of phase 1 droplets and phase 2 droplets are not synchronized. (B2 & B3) Both liquid phases are perturbed at the same frequency without a phase lag. As a result, the droplets have similar structures and the droplet size decreases with increasing perturbation frequency. f_1=f_2=(B2)20 Hz; (B3) 30 Hz. (B4, B5 & B6) Droplets are generated in the presence of perturbations with different frequencies(B4) f_1=20 Hz; f_2=10 Hz. Drop with two phase 1

droplet and one phase 2 droplets are generated. (B5) f_1=10 Hz; f_2=20 Hz. Drops with one phase 1 droplet and two phase 2 droplets are generated. (B6) f_1=10 Hz; f_2=30 Hz. Drops with one phase 1 droplet and three phase 2 droplets are generated. Scale bars are 200 μm.

The ability to precisely control the onset of the perturbation cycles allows the imposition of a phase lag between the two perturbations to the two droplet phases. We demonstrate that the phase lag can be manipulated to achieve different configurations of emulsion drops (Figure 7): while keeping the perturbation frequencies to be 10 Hz and 30 Hz, when the peak of the 30 Hz perturbation lags behind the peak of the 10 Hz one by 16 ms, the drops adopt a uniform multicompartmental structure of one phase 1 droplet and three phase 2 droplets (Figure 7 (A)); when the lag time of the peaks of the same perturbations decreases to around 0 ms, the configuration of drops becomes a train of drops with one phase 1 droplet and two phase 2 droplets, separated by a single phase 2 drop (Figure 7 (B)). A similar change in the configuration of drops can be observed when the lag time between a 10 Hz and a 20 Hz perturbation signals is varied, as shown in Figure 7 (C & D). The results illustrate the importance of controlling the lag time between perturbations when multiple perturbation cycles are applied, and also highlight the temporal precision of the perturbations achieved by the current approach.

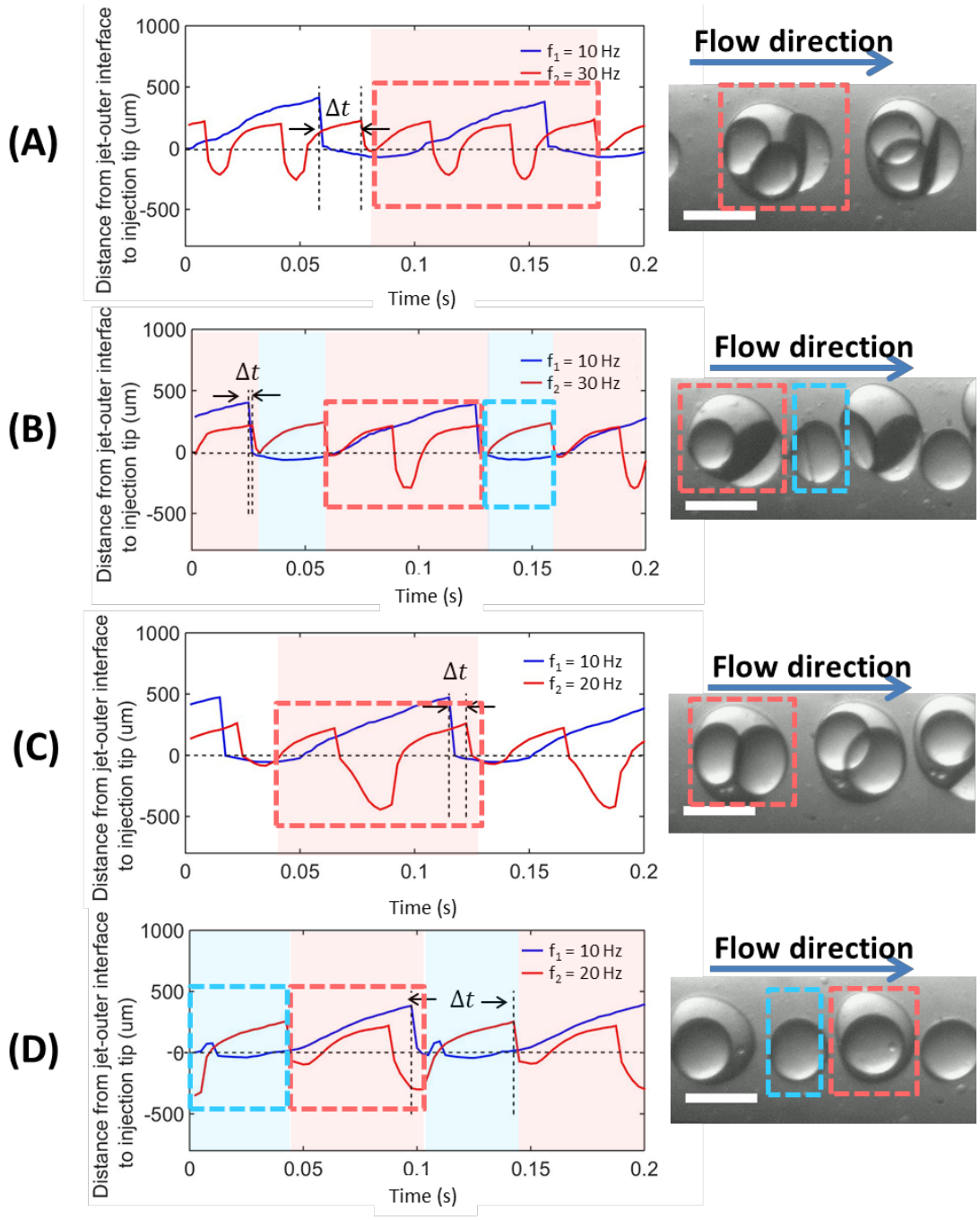

Figure 7 Droplet generation under two perturbation frequencies with different lag times. Scale bars are 200 µm. (A & B) 10 Hz and 30 Hz perturbations are imposed to phase 1 and phase 2 respectively, with different lag time Δt. (A) Δt = ~16 ms; this results in a continuous generation of drops with one phase 1 droplet and three phase 2 droplets; (B) Δt = ~0 ms; this results in a continuous generation of trains of drops with one phase 1 droplet and two phase 2 droplets, each

separated by a single phase 2 drop; 10 Hz and 20 Hz perturbations are imposed to phase 1 and phase 2 respectively, with different Δt. (C) Δt = ~10 ms; this results in a continuous generation of drops with one phase 1 droplet and two phase 2 droplets; (D) Δt = ~45 ms; this results in a continuous generation of trains of drops with one phase 1 droplet and one phase 2 droplet, each separated by a single phase 2 drop.

3.2.3 PiD approach for switching from single emulsion droplets to core-shell droplets during continuous operation

Apart from synchronization of multiple droplet generation steps, our PiD approach also allows direct manipulation of the structure of emulsion. For instance, to form droplets with a core-shell structure, in general, three phases are required: the inner and middle phases are for forming the core droplets and shell layers respectively, while the continuous phase helps to shear the liquid jets to break and attain the core-shell structure. However, using the PiD approach, these core-shell droplets can be prepared with a simple two-phase co-flow microfluidic geometry shown in Figure 8. By simply changing the wettability of the wall of the injection tip, the perturbation-induced approach can lead to the formation of droplets with core-shell structure. Using an injection tip with a hydrophilic inner wall and a hydrophobic outer wall, oil-in-water-in-oil emulsion droplets are prepared. Alternatively, using an injection tip with a hydrophobic inner wall– and a hydrophilic outer wall, water-in-oil-in-water droplets can also be generated. Using a jet phase of hexadecane and a continuous phase of 2 wt. % SDS solution, during the perturbation phase where the driving pressure is negative, both hexadecane and the aqueous phase retract upstream into the injection tip. Since the inner wall of the injection tip has been rendered hydrophobic in advance, it is wetted by hexadecane, but not the aqueous continuous phase, which form a curved interface, as schematically illustrated in Figure 8 (B1). As the negative

pressure decreases and gradually becomes positive, the neck that connects the aqueous phase in the injection capillary and that in the outside becomes thinner, as shown in Figure 8 (B2). Consequently, this triggers the breakup of the aqueous jet, resulting in an aqueous droplet in the hexadecane inside the injection capillary (Figure 8 (B3)). As the liquids are driven to flow downstream and exit the injection tip, the aqueous-droplet-containing hexadecane is pushed out of the injection tip, resulting in a water-in-oil-in-water double emulsion drop. The continuous periodic perturbation thus leads to the formation of a double emulsion droplet in each cycle, as shown in Figure 8 (C). By varying the amplitude of retraction, the sizes of inner core can be changed: The size of inner droplets increases with increasing amplitude of perturbation, as shown in Figure 8 (D). By taking the advantage of the retraction of fluid with each cycle of perturbation, our approach offers a way to generate droplets with a complicated structure using microfluidic devices with a relatively simple co-flow geometry.

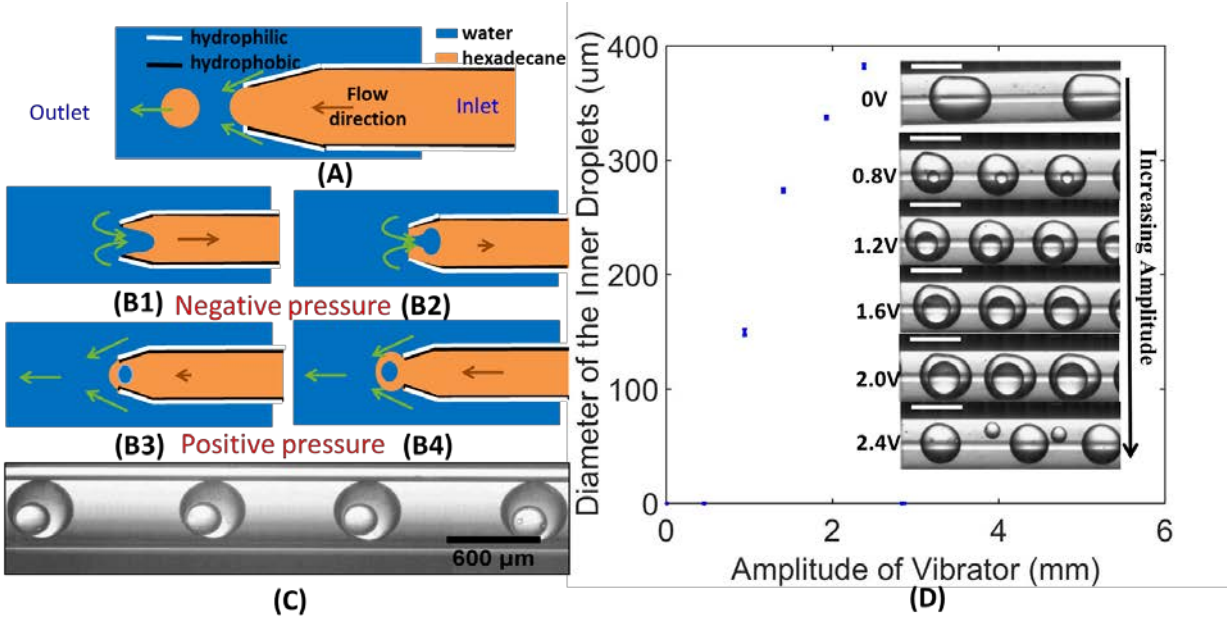

Figure 8 (A) Schematic diagram of droplets generation without perturbation. The inner glass wall is hydrophobic after being treated with octadecyl trimethoxysilane and the outer wall

remains hydrophilic without treatment. (B) Schematics of one-step generation of double emulsion induced by perturbation. (B1) Under negative pressure, the outer fluid is sucked back into the inner fluid resulting in the formation of a water jet inside hexadecane. (B2) The water jet breaks up into droplets following sufficient elongation inside hexadecane. (B3) Water droplets contained in hexadecane are pushed out from the injection tip when the driving pressure is positive. (B4) Hexadecane oil containing the water droplets breaks up into emulsion droplet, resulting in water-in-hexadecane-in-water double emulsion. (C) High-speed optical microscope image of the generated double emulsions. (D) High-speed optical microscope images of hexadecane-in-water-in-hexadecane double emulsion drops formed with different perturbation amplitudes. The size of the inner core of the double emulsion increases with increasing amplitude of perturbation. When the amplitude is too large, the core cannot be encapsulated and coalesce with the continuous phase. Scale bars are 600 μm.

4 CONCLUSION

Our approach of perturbation-induced droplet formation enables control over the droplet size and generation frequency, and is particularly effective when the perturbation amplitude is large and the interfacial tension is low. The response to the change in flow conditions towards the hydrodynamic perturbation is significantly faster than that triggered by changes in the flow rate using typical syringe pumps. Thus, it allows on-demand change in droplet sizes during continuous droplet generation. Besides the excellent control over the size of single emulsion droplets, the PiD approach also facilitates manipulating emulsion structure in continuous operation. By imposing varies frequencies to different droplet liquid phases, various bi-compartmental droplet structures can be realized. Besides, different phase lags of the imposed

perturbations further broaden the range of achievable droplet configurations. Besides multi-compartmental droplets with various structures, PiD approach can also realize the transform from single emulsion to core-shell droplets in a continuous operation.

Perturbation-induced droplet generation (PiD) approach creates new opportunities to customize the size distribution and synchronize parallel production of single emulsions; it also offers a new opportunity in generating droplets with on-demand structures.

ACKNOWLEDGEMENT

This research was supported by the Early Career Scheme (HKU 707712P) and the General Research Fund (HKU 719813E and 17304514) from the Research Grants Council of Hong Kong, the General Program (21476189/B060201) and Young Scholar's Program (NSFC51206138/E0605) from the National Natural Science Foundation of China, as well as the Seed Funding Programme for Basic Research (201211159090, 201311159105) and for Applied Research (201309160035) from the University of Hong Kong.

REFERENCES

1. Hsu, Y. H.; Lu, P.; Coleman, J.; Tang, W. A microfluidic platform to isolate avian erythrocytes infected with Plasmodium gallinaceum malaria parasites based on surface morphological changes. *Biomed Microdevices* **2011,** *13* (6), 995-1004.
2. Tan, J.; Du, L.; Lu, Y. C.; Xu, J. H.; Luo, G. S. Development of a gas–liquid microstructured system for oxidation of hydrogenated 2-ethyltetrahydroanthraquinone. *Chemical Engineering Journal* **2011,** *171* (3), 1406-1414.
3. Chen, Y.; Au, J.; Kazlas, P.; Ritenour, A.; Gates, H.; McCreary, M. Electronic paper: Flexible active-matrix electronic ink display. *Nature* **2003,** *423* (6936), 136-136.
4. Mason, B. P.; Price, K. E.; Steinbacher, J. L.; Bogdan, A. R.; McQuade, D. T. Greener Approaches to Organic Synthesis Using Microreactor Technology. *Chemical Reviews* **2007,** *107* (6), 2300-2318.

5. Liu, Z.; Shum, H. C. Fabrication of uniform multi-compartment particles using microfludic electrospray technology for cell co-culture studies. *Biomicrofluidics* **2013,** *7* (4), 044117.
6. Song, H.; Tice, J. D.; Ismagilov, R. F. A Microfluidic System for Controlling Reaction Networks in Time. *Angewandte Chemie* **2003,** *115* (7), 792-796.
7. Chow, A. H. L.; Tong, H. H. Y.; Chattopadhyay, P.; Shekunov, B. Y. Particle Engineering for Pulmonary Drug Delivery. *Pharmaceutical Research* **2007,** *24* (3), 411-437.
8. Gu, F. X.; Karnik, R.; Wang, A. Z.; Alexis, F.; Levy-Nissenbaum, E.; Hong, S.; Langer, R. S.; Farokhzad, O. C. Targeted nanoparticles for cancer therapy. *Nano Today* **2007,** *2* (3), 14-21.
9. DiCicco, M.; Neethirajan, S. An in vitro microfluidic gradient generator platform for antimicrobial testing. *BioChip J* **2014,** *8* (4), 282-288.
10. Fair, R. B. Digital microfluidics: is a true lab-on-a-chip possible? *Microfluid Nanofluid* **2007,** *3* (3), 245-281.
11. Wang, J. T.; Wang, J.; Han, J. J. Fabrication of Advanced Particles and Particle-Based Materials Assisted by Droplet-Based Microfluidics. *Small* **2011,** *7* (13), 1728-1754.
12. Min, N. G.; Kim, B.; Lee, T. Y.; Kim, D.; Lee, D. C.; Kim, S.-H. Anisotropic Microparticles Created by Phase Separation of Polymer Blends Confined in Monodisperse Emulsion Drops. *Langmuir* **2014,** *31* (3), 937-943.
13. Dendukuri, D.; Tsoi, K.; Hatton, T. A.; Doyle, P. S. Controlled Synthesis of Nonspherical Microparticles Using Microfluidics. *Langmuir* **2005,** *21* (6), 2113-2116.
14. Wheeler, A. R. Putting Electrowetting to Work. *Science* **2008,** *322* (5901), 539-540.
15. Srinivasan, V.; Pamula, V. K.; Fair, R. B. An integrated digital microfluidic lab-on-a-chip for clinical diagnostics on human physiological fluids. *Lab on a Chip* **2004,** *4* (4), 310-315.
16. Garstecki, P.; Fuerstman, M. J.; Stone, H. A.; Whitesides, G. M. Formation of droplets and bubbles in a microfluidic T-junction-scaling and mechanism of break-up. *Lab on a Chip* **2006,** *6* (3), 437-446.
17. Christopher, G. F.; Anna, S. L. Microfluidic methods for generating continuous droplet streams. *Journal of Physics D: Applied Physics* **2007,** *40* (19), R319.
18. Umbanhowar, P. B.; Prasad, V.; Weitz, D. A. Monodisperse Emulsion Generation via Drop Break Off in a Coflowing Stream. *Langmuir* **1999,** *16* (2), 347-351.
19. Baroud, C. N.; Gallaire, F.; Dangla, R. Dynamics of microfluidic droplets. *Lab on a Chip* **2010,** *10* (16), 2032-2045.
20. Utada, A. S.; Fernandez-Nieves, A.; Stone, H. A.; Weitz, D. A. Dripping to Jetting Transitions in Coflowing Liquid Streams. *Physical Review Letters* **2007,** *99* (9), 094502.
21. Thorsen, T.; Roberts, R. W.; Arnold, F. H.; Quake, S. R. Dynamic Pattern Formation in a Vesicle-Generating Microfluidic Device. *Physical Review Letters* **2001,** *86* (18), 4163-4166.
22. Nie, Z.; Seo, M.; Xu, S.; Lewis, P.; Mok, M.; Kumacheva, E.; Whitesides, G.; Garstecki, P.; Stone, H. Emulsification in a microfluidic flow-focusing device: effect of the viscosities of the liquids. *Microfluid Nanofluid* **2008,** *5* (5), 585-594.
23. Xu, J. H.; Li, S. W.; Tan, J.; Wang, Y. J.; Luo, G. S. Preparation of highly monodisperse droplet in a T-junction microfluidic device. *AIChE Journal* **2006,** *52* (9), 3005-3010.
24. Hong, Y.; Wang, F. Flow rate effect on droplet control in a co-flowing microfluidic device. *Microfluid Nanofluid* **2007,** *3* (3), 341-346.
25. Anna, S. L.; Bontoux, N.; Stone, H. A. Formation of dispersions using “flow focusing” in microchannels. *Applied Physics Letters* **2003,** *82* (3), 364-366.

26. Ward, T.; Faivre, M.; Abkarian, M.; Stone, H. A. Microfluidic flow focusing: Drop size and scaling in pressure versus flow-rate-driven pumping. *ELECTROPHORESIS* **2005,** *26* (19), 3716-3724.
27. Stone, H. A.; Stroock, A. D.; Ajdari, A. ENGINEERING FLOWS IN SMALL DEVICES: Microfluidics Toward a Lab-on-a-Chip. *Annual Review of Fluid Mechanics* **2004,** *36* (1), 381-411.
28. Gupta, A.; Kumar, R. Effect of geometry on droplet formation in the squeezing regime in a microfluidic T-junction. *Microfluid Nanofluid* **2010,** *8* (6), 799-812.
29. Cramer, C.; Fischer, P.; Windhab, E. J. Drop formation in a co-flowing ambient fluid. *Chemical Engineering Science* **2004,** *59* (15), 3045-3058.
30. Okushima, S.; Nisisako, T.; Torii, T.; Higuchi, T. Controlled Production of Monodisperse Double Emulsions by Two-Step Droplet Breakup in Microfluidic Devices. *Langmuir* **2004,** *20* (23), 9905-9908.
31. Utada, A. S.; Lorenceau, E.; Link, D. R.; Kaplan, P. D.; Stone, H. A.; Weitz, D. A. Monodisperse Double Emulsions Generated from a Microcapillary Device. *Science* **2005,** *308* (5721), 537-541.
32. Chu, L.-Y.; Utada, A. S.; Shah, R. K.; Kim, J.-W.; Weitz, D. A. Controllable Monodisperse Multiple Emulsions. *Angewandte Chemie International Edition* **2007,** *46* (47), 8970-8974.
33. Li, Z.; Mak, S. Y.; Sauret, A.; Shum, H. C. Syringe-pump-induced fluctuation in all-aqueous microfluidic system implications for flow rate accuracy. *Lab on a Chip* **2014,** *14* (4), 744-749.
34. Zhou, H.; Yao, S. A facile on-demand droplet microfluidic system for lab-on-a-chip applications. *Microfluid Nanofluid* **2014,** *16* (4), 667-675.
35. Bransky, A.; Korin, N.; Khoury, M.; Levenberg, S. A microfluidic droplet generator based on a piezoelectric actuator. *Lab on a Chip* **2009,** *9* (4), 516-520.
36. Chong, Z. Z.; Tor, S. B.; Loh, N. H.; Wong, T. N.; Ganan-Calvo, A. M.; Tan, S. H.; Nguyen, N.-T. Acoustofluidic control of bubble size in microfluidic flow-focusing configuration. *Lab on a Chip* **2015,** *15* (4), 996-999.
37. Churski, K.; Michalski, J.; Garstecki, P. Droplet on demand system utilizing a computer controlled microvalve integrated into a stiff polymeric microfluidic device. *Lab on a Chip* **2010,** *10* (4), 512-518.
38. Yogi, O.; Kawakami, T.; Yamauchi, M.; Ye, J. Y.; Ishikawa, M. On-Demand Droplet Spotter for Preparing Pico- to Femtoliter Droplets on Surfaces. *Analytical Chemistry* **2001,** *73* (8), 1896-1902.
39. Sauret, A.; Shum, H. C. Forced generation of simple and double emulsions in all-aqueous systems. *Applied Physics Letters* **2012,** *100* (15), 154106.
40. James, A. J.; Smith, M. K.; Glezer, A. Vibration-induced drop atomization and the numerical simulation of low-frequency single-droplet ejection. *Journal of Fluid Mechanics* **2003,** *476*, 29-62.
41. Yule, A. J.; Al-Suleimani, Y. On Droplet Formation from Capillary Waves on a Vibrating Surface. *Proceedings: Mathematical, Physical and Engineering Sciences* **2000,** *456* (1997), 1069-1085.
42. Shum, A. S. H. C. Beating the Jetting Regime. In *international Journal of Nonlinear Sciences and Numerical Simulation*, 2012; Vol. 13, pp 351-362.

43. Brünahl, J.; Grishin, A. M. Piezoelectric shear mode drop-on-demand inkjet actuator. *Sensors and Actuators A: Physical* **2002,** *101* (3), 371-382.
44. Song, Y.; Sauret, A.; Cheung Shum, H. All-aqueous multiphase microfluidics. *Biomicrofluidics* **2013,** *7* (6), 061301.
45. Guo, F.; Liu, K.; Ji, X. H.; Ding, H.-J.; Zhang, M.; Zeng, Q.; Liu, W.; Guo, S.-S.; Zhao, X.-Z. Valve-based microfluidic device for droplet on-demand operation and static assay. *Applied Physics Letters* **2010,** *97* (23), 233701.
46. Wixforth, A.; Strobl, C.; Gauer, C.; Toegl, A.; Scriba, J.; v. Guttenberg, Z. Acoustic manipulation of small droplets. *Analytical & Bioanalytical Chemistry* **2004,** *379* (7/8), 982-991.
47. Schmid, L.; Franke, T. Acoustic modulation of droplet size in a T-junction. *Applied Physics Letters* **2014,** *104* (13), 133501.
48. Song, Y.; Shum, H. C. Monodisperse w/w/w Double Emulsion Induced by Phase Separation. *Langmuir* **2012,** *28* (33), 12054-12059.
49. Ding, Y.; Casadevall i Solvas, X.; deMello, A. "V-junction": a novel structure for high-speed generation of bespoke droplet flows. *Analyst* **2015,** *140* (2), 414-421.
50. Zeng, S.; Li, B.; Su, X. o.; Qin, J.; Lin, B. Microvalve-actuated precise control of individual droplets in microfluidic devices. *Lab on a Chip* **2009,** *9* (10), 1340-1343.
51. Geschiere, S. D.; Ziemecka, I.; van Steijn, V.; Koper, G. J. M.; Esch, J. H. v.; Kreutzer, M. T. Slow growth of the Rayleigh-Plateau instability in aqueous two phase systems. *Biomicrofluidics* **2012,** *6* (2), 022007-022007-11.